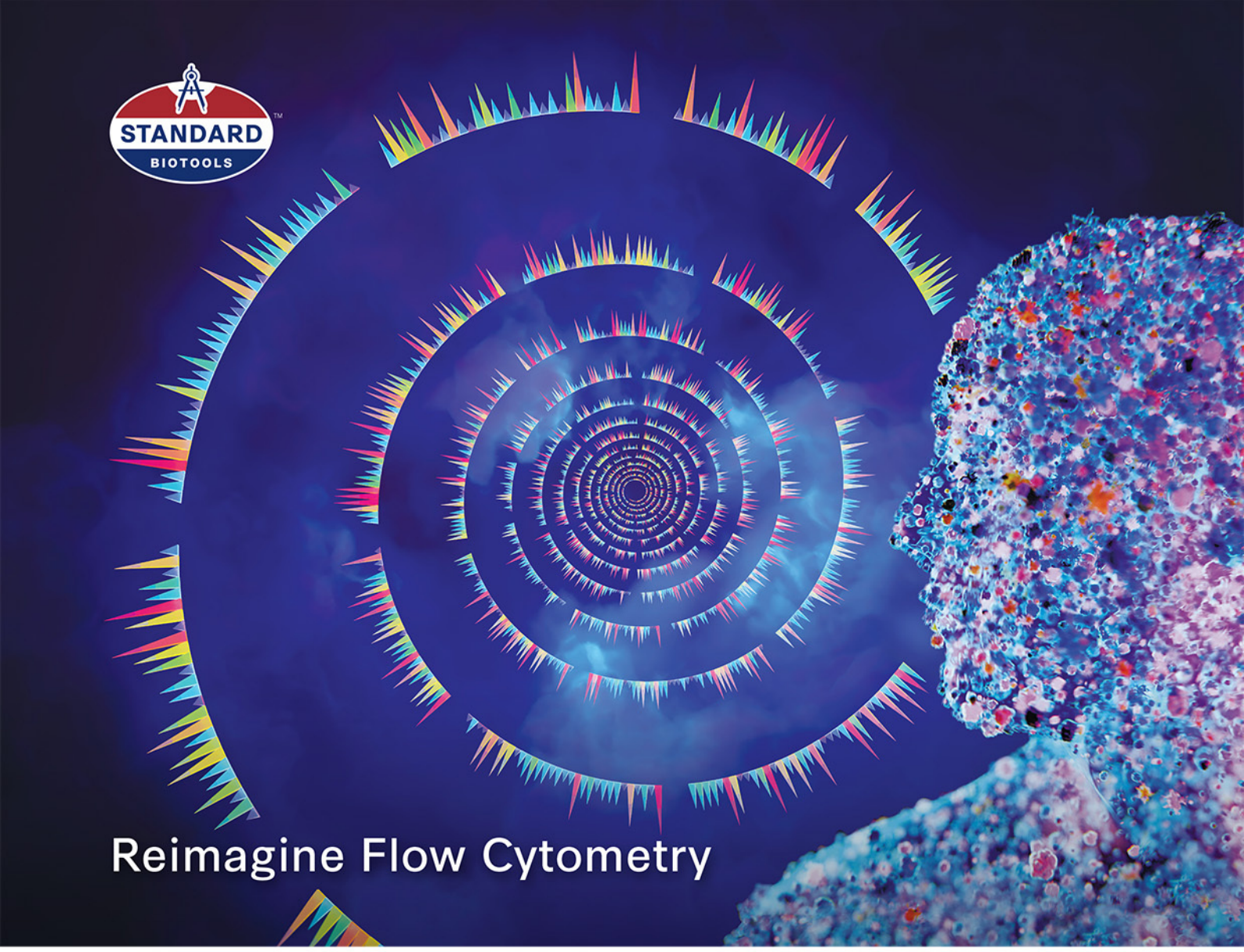

Tired of repetitive rounds of panel design and validation?

Want to optimize your time and get the most out of your precious samples?

Try one of our eight ready-to-go 40+ marker panels for deep immune profiling.

From a total of only 300 µL whole blood or 3 x 10^6 PBMC, you can

- Identify all major T, B, NK and myeloid populations
- Measure their activation status, cytokine production and cytotoxic capability
- Get your results in a single day using an automated data analysis solution
- Stain, freeze, store and ship samples if needed

Learn more about the family of **Maxpar®** **Direct™ Immune Profiling** panels today >

For Research Use Only. Not for use in diagnostic procedures.

Received: 31 May 2022 | Revised: 9 July 2022 | Accepted: 21 July 2022

DOI: 10.1002/cyto.a.24675

ORIGINAL ARTICLE

ISAC CYTOMETRY Journal of Quantitative Cell Science PART A

Taking molecular pathology to the next level: Whole slide multicolor confocal imaging with the Pannoramic Confocal digital pathology scanner

István Rebenku[1,2] | Ferenc A. Bartha[3] | Tamás Katona[1,4] | Barbara Zsebik[1,2,5] | Géza Antalffy[6] | Lili Takács[7] | Béla Molnár[6,8,9] | György Vereb[1,2]

[1]Department of Biophysics and Cell Biology, Faculty of Medicine, University of Debrecen, Debrecen, Hungary

[2]ELKH-DE Cell Biology and Signaling Research Group, Faculty of Medicine, University of Debrecen, Debrecen, Hungary

[3]Bolyai Institute, University of Szeged, Szeged, Hungary

[4]Department of Data Science and Visualization, Faculty of Informatics, University of Debrecen, Debrecen, Hungary

[5]Department of Biopharmacy, Faculty of Pharmacy, University of Debrecen, Debrecen, Hungary

[6]3DHISTECH Ltd., Budapest, Hungary

[7]Department of Ophthalmology, Faculty of Medicine, University of Debrecen, Debrecen, Hungary

[8]Department of Internal Medicine and Oncology, Semmelweis University, Budapest, Hungary

[9]Molecular Medicine Research Group, Eötvös Loránd Research Network, Budapest, Hungary

Correspondence
Béla Molnár, Department of Internal Medicine and Oncology, Semmelweis University, Korányi u. 2/a., H-1083 Budapest, Hungary.
Email: bela.molnar@3dhistech.com

György Vereb, Department of Biophysics and Cell Biology, Faculty of Medicine, University of Debrecen, Egyetem tér 1, H-4032 Debrecen, Hungary.
Email: gvereb2020@gmail.com

Funding information
the National Research, Development and Innovation Office, Hungary, Grant/Award Number: OTKA K135938; European Regional Development Fund, Grant/Award Number: GINOP-2.2.1-15-2017-00072

Abstract

The emergence and fast advance of digital pathology allows the acquisition, digital storage, interactive recall and analysis of morphology at the tissue level. When applying immunohistochemistry, it also affords the correlation of morphology with the expression of one or two specific molecule of interest. The rise of fluorescence pathology scanners expands the number of detected molecules based on multiplex labeling. The Pannoramic Confocal (created by 3DHistech, Hungary) is a first-of-the-kind digital pathology scanner that affords not only multiplexed fluorescent detection on top of conventional transmission imaging, but also confocality. We have benchmarked this scanner in terms of stability, precision, light efficiency, linearity and sensitivity. X–Y stability and relocalisation precision were well below resolution limit (≤50 nm). Light throughput in confocal mode was 4–5 times higher than that of a point scanning confocal microscope, yielding similar calculated confocal intensities but with the potential for improving signal to noise ratio or scan speed. Response was linear with $R^2 \geq 0.9996$. Calibrated measurements showed that using indirect labeling ≥2000 molecules per cell could be well detected and imaged on the cell surface. Both standard-based and statistical post-acquisition flatfield corrections are implemented. We have also measured the point spread function (PSF) of the instrument. The dimensions of the PSF are somewhat larger and less symmetric than of the theoretical PSF of a conventional CLSM, however, the spatial homogeneity of these parameters allows for obtaining a specific system PSF for each optical path and using it for optional on-the-fly deconvolution. In conclusion, the Pannoramic Confocal provides sensitive, quantitative widefield and confocal detection of multiplexed fluorescence signals, with optical sectioning and 3D reconstruction, in addition to brightfield transmission imaging. High speed scanning of large samples, analysis of tissue heterogeneity, and detection of rare events open up new ways for quantitatively analyzing tissue sections, organoid cultures or large numbers of adherent cells.

KEYWORDS
3-dimensional virtual slide, deconvolution, digital pathology, multispectral fluorescence imaging, widefield aperture correlated confocal imaging

1 | INTRODUCTION

Digital pathology is becoming mainstream in routine diagnostics. This includes but is not limited to nephropathology [1] and tissue biomarker research [2]. This development is enabled by whole side scanners becoming faster, and by the increase of the affordability of storage place and computational power [3]. Most routine diagnostic fields currently use bright field methods.

Fluorescence imaging, especially confocal image formation is an emerging field of automated whole slide scanning. Even in the 2021 issue of the European Society of Digital and Integrative Pathology's best practice recommendation for digital pathology, fluorescent methods are only mentioned but not discussed [4]. Meanwhile there are many fluorescent techniques in development or waiting to enter the daily routine of digital pathology or scientific discovery [5]. Introducing confocality to automatic image acquisition instruments can improve image quality and dramatically increase depth resolution, which enables the use of techniques previously not feasible with whole slide scanners, such as 3D FISH [6]. Digital pathology and whole slide scanning is a continuously improving field, where benchmarking novel instrumentation and quality control are essential for ensuring high standards.

The Pannoramic Confocal is a confocal fluorescence slide scanner. The confocal image formation of the microscope is provided by an Aurox cc88 aperture correlation confocal imaging system (see Figure 1 for optical design). The spinning disk has a grid pattern of transmitting and reflective regions on its surface, which modulates the excitation light coming from a Lumencor multispectral light source (for spectral properties see Table 1), and demodulates the emission. The emitted light is split by the spinning disk to transmitted and reflected light, each imaged onto one of the halves of a single sCMOS camera chip (pco.edge 5.5 with 2560 × 2160 resolution 6.5 × 6.5 μm physical pixel size, >60% quantum efficiency). The reflected image is made up of a random half of photons originating from nonconjugate planes, while the other half of these photons and those from the conjugate plane constitute the transmitted image. Thus, as illustrated in Figure 1, the transmitted (I_T) and reflected (I_R) images can be used to calculate the confocal (I_C) and the widefield (I_W) images using:

$$I_W = I_T + kI_R$$

$$I_C = I_T - kI_R$$

where k is an experimental correction factor (~0.9), accounting for the lesser light loss on reflective surfaces as opposed to the transmitted light. This factor represents the optical characteristics of not only the spinning disk, but also of the light paths of transmitted and reflected images beyond the spinning disk all the way to the camera. As such, it is stable in time, but may exhibit small variations from device to device and therefore the manufacturer provides its value for each device. Using the built-in calibration light source, the value of k can be verified using the raw image grabbed by the camera.

When the spinning disk is removed from the light path, the microscope operates as a conventional epifluorescence microscope in widefield mode. Additionally, brightfield images can also be acquired. Slides are automatically fed from a 10-slot tray and imaged through

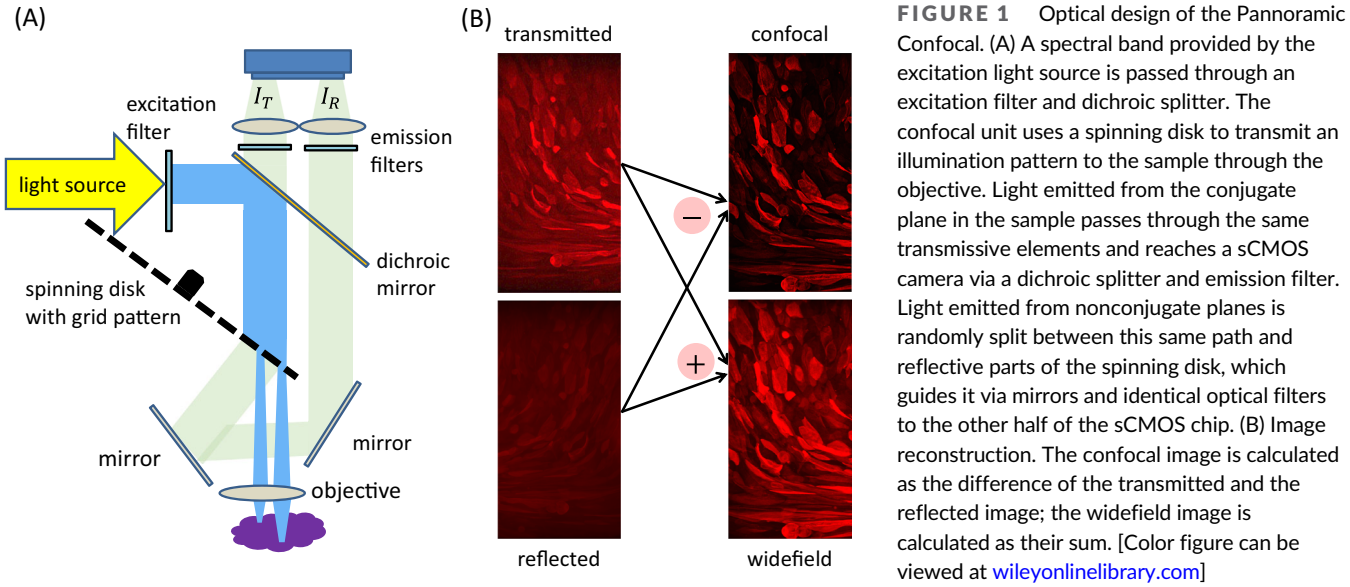

FIGURE 1 Optical design of the Pannoramic Confocal. (A) A spectral band provided by the excitation light source is passed through an excitation filter and dichroic splitter. The confocal unit uses a spinning disk to transmit an illumination pattern to the sample through the objective. Light emitted from the conjugate plane in the sample passes through the same transmissive elements and reaches a sCMOS camera via a dichroic splitter and emission filter. Light emitted from nonconjugate planes is randomly split between this same path and reflective parts of the spinning disk, which guides it via mirrors and identical optical filters to the other half of the sCMOS chip. (B) Image reconstruction. The confocal image is calculated as the difference of the transmitted and the reflected image; the widefield image is calculated as their sum. [Color figure can be viewed at wileyonlinelibrary.com]

either a 20× Plan-Apochromat (NA = 0.8) item no.: 420650-9901 Carl Zeiss Jena or a 40× C-Apochromat water immersion (NA = 1.2) item no.: 421767-9971 objective. In the tested configuration, these objectives were from Carl Zeiss, Jena, Germany. Replenishment of immersion water is automatic.

We have benchmarked this scanner in terms of confocal performance, stability, precision, light efficiency, sensitivity and linearity, and applicability to study large and thick samples with multifluorescent labeling.

2 | MATERIALS AND METHODS

All reagents not specified otherwise were obtained from Sigma-Aldrich, St. Louis, MO, USA.

2.1 | Point source beads

PS-Speck beads (Thermo Fisher/Invitrogen Cat# P7220) were mounted on poly-L-lysine coated coverslips. Rectangle coverslips (24 × 40 mm, Thermo Fisher) were degreased with acetone and put into 1 mg/ml poly-L-Lysine solution for 2 h and dried. Two microliters of the PS-Speck stock solution was measured into 500 µl 1% BSA in distilled water, the bead solution pipetted onto the dried coverslips and spread with a pipette tip. The beads dried on the coverslip and were mounted in Mowiol antifade (0.1 M TrisHCl, pH 8.5, 25% [w/v] glycerol, and 10% Mowiol 4-88, Polysciences, Warrington, PA, USA). Tetraspeck 0.5 µm beads (Thermo Fisher/Invitrogen Cat# T7281) were mounted in the same way onto degreased coverslips, using 5 µl of stock solution. In this case, no poly-L-lysine coating was necessary for sample stability.

2.2 | Cell culture and fluorescent labeling

A172 glioblastoma cells (ATCC Cat# CRL-1620) were cultured in DMEM supplemented with 10% FBS, at 37°C with 5% CO_2 in a humidified incubator for 2 days on sterilized 25 mm diameter round glass coverslips (0.17 mm thickness). 100 nM Mito Tracker Red (Thermo Fisher) in DMEM supplemented with 10% FBS was added 20 min prior to immunofluorescent labeling of the cell culture. Cells were washed three times on ice with HEPES buffer supplemented with 4 mM glucose (HEPES/Glucose). The primary antibody was mAb TS2/16.2.1, an anti-integrin β1, produced in-house from hybridoma (ATCC Cat# HB-243). This was diluted to 10 µg/ml in HEPES/Glucose and added to cells on ice for 25 min, then washed off three times with HEPES/Glucose. The samples were fixed for 3 min with acetone on ice, and then labeled for 25 min in HEPES buffer containing 5 µg/ml goat anti-mouse IgG conjugated with Alexa Fluor 647, 0.5 µg/ml DAPI, and 0.5 µg/ml FITC-phalloidin. Cells were then washed three times and mounted in Mowiol antifade.

2.3 | 3D cell multilayer model

Cell multilayers of conjuctival origin were generated as described in detail in References [7, 8] (ethical permit number: IX-R-052/00016-28/2012). The contact lenses carrying the cell multilayer were immunostained at room temperature as follows. After increasing concentration of acetone (10%, 20%, 40%, 70%, and 100%) and washing, samples were permeabilized and blocked with PBS containing 2% BSA and 0.1% Triton X-100 for 1 h. The samples were incubated with primary antibodies for 1.5 h using the following concentrations:

20 µg/ml Alexa Fluor 647 anti-cytokeratin 19 (Abcam) (EPR1579Y) (ab205446); 5 µg/ml guinea pig anti-CK3 (Fitzgerald, Acton, MA, USA, Cat# 20R-2642), and 5 µg/ml Cy3 conjugated mouse anti-vimentin (Sigma Aldrich, Cat# C9080, clone V9). After washing three times with PBS/0.05% Triton X-100, samples were incubated with 1 µg/ml fluorophore-conjugated, highly cross-absorbed secondary antibodies: donkey anti-guinea pig-Alexa Fluor 488 (Jackson ImmunoResearch, West Grove, PA, USA, Cat# 706-545-148). Nuclei were counterstained with 0.01 mg/ml DAPI during the second wash step, then samples were fixed with 1% formaldehyde in PBS for 10 min, rinsed and mounted in Mowiol. Autofluorescence and FMO controls were also prepared.

2.4 | Laser scanning confocal microscopy

Comparative measurements of light efficiency, and of large 3D samples was done with a confocal laser scanning microscope (LSM 880, Carl Zeiss GmbH, Jena, Germany) using a 40× C-Apochromat water immersion objective (NA = 1.2, item no.: 421767-9971). DAPI was excited at 405 nm, Alexa Fluor 488 at 488 nm, Cy3 at 543 nm, and Alexa Fluor 647 at 633 nm. Their fluorescence emission was

TABLE 1 Spectral characteristics of light sources and the filters used in the Pannoramic Confocal

Channel	Excitation light	Excitation filter	Dichroic mirror	Emission filter
DAPI	386/23	392/23	409	447/60
(CFP)	438/24			
FITC	475/28	474/27	495	525/45
(YFP)	512/25			
TRITC	550/88	543/22	562	593/40
Cy5	650/13	628/32	652	680/42

spectrally resolved onto a 32 element GaAsP array optimizing detection bands for minimal crosstalk in sequential excitation (multitrack mode). Optimal Nyquist sampling was done through either fully open or 1-Airy-Unit-sized pinholes.

2.5 | Filters used in the Pannoramic Confocal

The exact specifications of applied optical filter sets for all measurements are listed in Table 1.

2.6 | Characterization of the system PSF and deconvolution

The experimental PSF was determined with PS Speck point source beads. One hundred slices with 200 nm Z step were taken in every channel of the microscope. For the 20× objective, maximum excitation intensity and 2000 ms exposure times were used for the DAPI and CY5 channels, while for the 40× objective maximum excitation intensity and 200 ms exposure times were used in every channel. The PSF symmetry distribution map and theoretical PSF dimensions were constructed with PSFj [9]. Symmetry was defined as the ratio of the smallest and the largest lateral half widths. For experimentally deriving the actual PSF, the Huygens software (SVI, NL) was used. In every channel, 25 beads were cropped and averaged and the PSF was reconstructed from the averaged beads. The biological samples were imaged with 100% excitation intensity and 20 ms exposure time in the DAPI channel and 200 ms exposure times in every other channel. The deconvolution was done with the Huygens Classic Maximum Likelihood Estimation (CMLE) algorithm, limited to maximum 50 iterations.

2.7 | Stability and relocalisation precision

TetraSpeck beads (500 nm) were imaged with the Pannoramic Confocal in widefield imaging mode. Stability was measured on 120 consecutive images, taken over a 2-h period. For measuring the relocalisation precision, 10 consecutive images were taken, and between each exposure, the stage was moved away and back by one field of view, and this was repeated along both translation axes in both directions. The movement of 15 individual beads was tracked with the TrackMate [10]. Plugin in FIJI, and the mean dislocation ± SD was plotted. To facilitate the thermal equilibrium of the system, the room was air conditioned, and a fan was used to promote the redistribution of cooled air.

2.8 | Measurement of illumination homogeneity

The homogeneity of illumination was measured by imaging a blue excitation fluorescence reference slide (Ted Pella, Redding, CA, USA, Fluor-Ref, Prod#: 2273). For the 20× objective, the DAPI, FITC, TRITC, and Cy5 channels were imaged using the following exposure times and excitation intensities, respectively: 20 ms/4%, 20 ms/70%, 100 ms/100%, and 20 ms/50%. For the 40× objective, the corresponding data were 20 ms/8%, 40 ms/100%, 300 ms/100%, and 60 ms/100%. Twenty images were captured for every channel and averaged to decrease noise.

2.9 | Linearity measurement

The linearity of instrument response was measured using InSpeck green linearity calibration beads (ThermoFisher, Cat# I14785) containing six bead populations of different intensity. The beads were imaged in 15 focal planes 1.2 μm apart. Exposure time and excitation power were 160 ms/100% in the TRITC channel in widefield mode, and 20 ms/4% in the FITC channel in confocal mode. Shifting the channels between the two modes was necessary to image the whole intensity range with the same exposure time and illumination. Focal planes were average Z projected, and the average background was subtracted. Individual bead intensities were measured and averaged in both widefield and confocal imaging mode.

2.10 | Assessing instrument sensitivity

Sensitivity was determined by using QIFIKIT calibration beads containing five bead populations with different numbers of mouse antibody FC regions conjugated to their surface (2200; 14,000; 48,000; 169,000; 724,000 in the batch used). Thirty microliters of calibration beads was labeled with 10 μg/ml goat anti-mouse IgG conjugated with Alexa Fluor 488 in HEPES buffer for 20 min in a sorter tube, washed with 3 ml buffer and centrifuged at 300*g* for 5 min. The supernatant was discarded, and the beads were resuspended in 100 μl HEPES buffer. The bead suspension was dried on the coverslip overnight, then mounted in Mowiol antifade. The sample was imaged with 100% excitation intensity and 20 ms exposure time in widefield mode and 600 ms exposure time in confocal mode. The background was subtracted and 1190 beads were measured in widefield mode, and 3196 in confocal mode.

2.11 | Measuring light efficiency parameters

Excitation intensities were determined at several points in the optical path with a Thor labs s170C microscope slide power sensor set to 365, 488, 543, and 633 nm for the DAPI, FITC, TRITC, and Cy5 channels, respectively. Light loss through the objectives and the spinning disk was calculated. For assessing emitted light, 1 μm beads of the FocalCheck Fluorescence Microscope Test Slide #1 (Thermo Fisher/Molecular Probes Cat# F36909) were imaged with the Pannoramic Confocal, and for reference, with a Zeiss LSM 880 microscope. Thirty focal planes were acquired with 200 nm steps between them, the background subtracted, and the average intensity of the beads determined and compared across microscopes and various imaging modes.

TABLE 2 Dimensions of the measured PSF with SD and the corresponding theoretical values for a laser scanning confocal microscope for the case of the 40× water immersion objective

20×	Measured PSF dimension (nm)				Theoretical PSF (nm)			
FWHM	DAPI	FITC	TRITC	Cy5	DAPI	FITC	TRITC	Cy5
X	749 ± 103	733 ± 88	846 ± 85	842 ± 112	267	330	365	423
Y	579 ± 82	716 ± 84	831 ± 44	866 ± 46				
Z	2007 ± 212	4103 ± 244	4749 ± 288	4836 ± 367	1150	1420	1570	1810
Symmetry	0.852 ± 0.00	0.871 ± 0.035	0.899 ± 0.026	0.931 ± 0.00	1	1	1	1
40×	Measured PSF dimension (nm)				Theoretical PSF (nm)			
FWHM	DAPI	FITC	TRITC	Cy5	DAPI	FITC	TRITC	Cy5
X	529 ± 10	586 ± 13	702 ± 19	611 ± 24	184	218	252	282
Y	363 ± 18	423 ± 20	439 ± 24	592 ± 12				
Z	1640 ± 108	2326 ± 72	2560 ± 145	2649 ± 54	699	829	959	1070
Symmetry	0.673 ± 0.03	0.697 ± 0.055	0.702 ± 0.027	0.714 ± 0.019	1	1	1	1

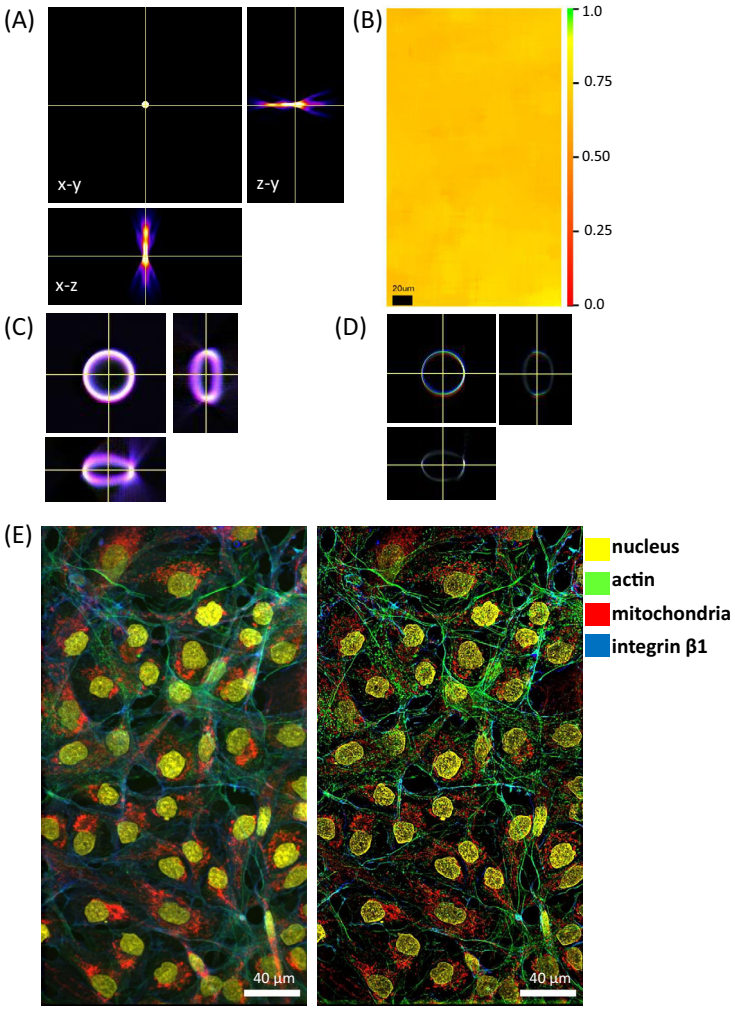

FIGURE 2 Confocal performance. (A) Orthogonal projection of the measured system PSF. (B) Spatial distribution of PSF symmetry. (C) Orthogonal projection of a 15 µm surface-stained bead. (D) Deconvolved image of the bead in (C) using the measured PSF from (A). (E) Z-projection (average intensity mode, Fiji) of a 4-channel confocal stack, original on the left, and after deconvolution on the right. The 40× water immersion (NA = 1.2) was used. Forty confocal slices were acquired with a Z step of 400 nm. 3D rendering (mean value mode, interpolated, with 1° increments, Fiji) can be viewed as Video S1. The upper and lower five slices of the stack are not displayed. [Color figure can be viewed at wileyonlinelibrary.com]

3 | RESULTS AND DISCUSSION

3.1 | Confocal performance

As shown in Table 2, the measured PSF of the Pannoramic Confocal is larger in every dimension compared to the theoretical value of a conventional laser scanning microscope, with both the studied objectives. The measured PSF is not symmetric (Figure 2A). This characteristic of the PSF makes it impossible to use a theoretical PSF for deconvolution. However, the PSF symmetry shows a spatially homogeneous distribution (Figure 2B), which makes possible the use of a single empirical PSF for each channel. Deconvolution was tested on a

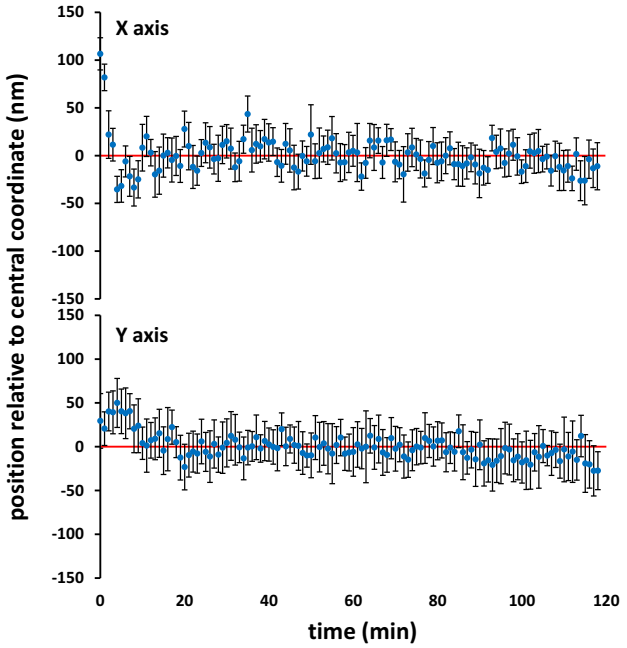

FIGURE 3 Instrument stability. The same field of view of 500 nm beads was imaged once every minute for 2 h. The movement of individual beads was tracked, and the dislocation of each bead at every time point from its own central position was calculated and plotted as mean ± SD for 15 beads. [Color figure can be viewed at wileyonlinelibrary.com]

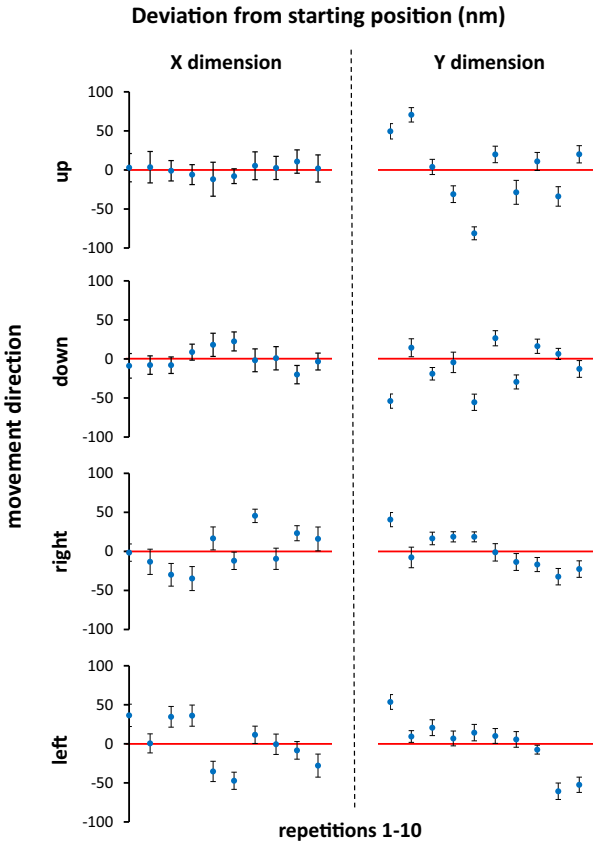

FIGURE 4 Precision of relocalisation. The same field of view of 500 nm beads was imaged 10 times, and between each exposure the stage was moved away and back by one field of view. This was repeated along both translation axes in both directions. The movement of individual beads was tracked, and the dislocation of each bead at every time point from its own initial position was calculated and plotted as mean ± SD for 15 beads. [Color figure can be viewed at wileyonlinelibrary.com]

single 15 μm surface-stained bead (Figure 2C,D), and on confluent A172 glioblastoma cells grown on a coverslip, stained with four fluorescent dyes to assess the efficacy of deconvolution in four fluorescent channels simultaneously (Figure 2E, Video S1). Deconvolution visibly decreased the blurriness of the images. On the images of beads, deconvolution resulted in a fine, approximately one-pixel thick ring, corresponding to the expectations. In the case of cellular samples, deconvolution increased the discernibility of the fine structures inside the cells. The current acquisition program includes the option for on-the-fly deconvolution using the system PSF stored for each optical path separately.

3.2 | Stability and relocalisation

Stage stability was measured by taking images of 0.5 μm Tetraspeck beads in every minute for 2 h, with the 20× magnification objective. We have tracked the movement of 15 beads with the FIJI TrackMate plugin. As Figure 3 shows, we detected a slight subpixel (<325 nm) movement in the beginning of the experiment which has decreased to negligible in 10 min, possibly owed to reaching thermal equilibrium by the sample and the stage. To measure the relocalization precision of the instrument we have taken images after moving the sample back and forth in the given direction. After 10 repetitions, the position of the beads was determined with the FIJI TrackMate plugin. Differences in the relocalization positions are shown in Figure 4. The dislocation in each direction was smaller than the size of a pixel in every case. Also, the larger deviations were manifested along the axis of displacement, with the orthogonal axis relatively unaffected.

3.3 | Illumination and light efficiency of the microscope

Excitation light intensities were measured in every channel and image formation mode result shown in Table 3A. The highest excitation light intensity was measured in the TRITC channel, the peak quantum efficiency of the camera also at the TRITC channel. This result indicates the highest sensitivity that can be achieved in the TRITC channel. The light loss on the optical elements shows a small wavelength dependence (Table 3B). The spinning disk transmits 44%–47% of the light. The 20× magnification objective has a 91%–98% transmission, while the 40× objective due to the higher number of optical elements transmits 32%–34% of the entering light. The light efficiencies of the whole imaging system in different imaging modes were determined and compared to each other and to a Carl Zeiss LSM 880 microscope (Table 3C). In restored widefield mode, 29%–36% of the intensities obtained without the

TABLE 3 Intensity of excitation light sources, and light efficiency of the Pannoramic Confocal

(A) Maximum excitation light intensities (mW)				
	20× objective		40× objective	
	Widefield	Confocal	Widefield	Confocal
DAPI	9.3	4.1	3.3	1.51
FITC	69.3	31.1	24.1	11.2
TRITC	92.1	41.5	31	14.2
Cy5	62.1	27.4	21.3	9.9
(B) Excitation light efficiency (% remaining)				
	Spinning disk		Objective	
	For 20× objective	For 40× objective	20× objective	40× objective
DAPI	44.2%	46.0%	91.3%	32.3%
FITC	44.9%	46.5%	97.6%	34.0%
TRITC	45.1%	45.8%	93.9%	31.6%
Cy5	44.1%	46.6%	92.8%	31.8%
(C) Relative light efficiency in various imaging modes (% remaining)				
	Pannoramic Confocal		Reference: Zeiss LSM 880	
	Restored WF/WF	Confocal/ WF	1 Airy unit pinhole/open pinhole	
FITC	33.7%	4.3%	4.1%	
TRITC	35.9%	4.2%	4.8%	
Cy5	29.4%	4.1%	3.3%	

spinning disk (true widefield mode) were measured, whereas in confocal mode, 4.1%–4.3% of the true widefield intensity was measured. In the CLSM, the intensity remaining with a 1 Airy unit pinhole setting compared to the open pinhole case was in a similar range (3.3%–4.8%). It may be noted, however, that the measured intensities used for calculating the confocal image are 4–5 times higher than those measured in the confocal microscope, and therefore could afford an overall better signal to noise ratio or a faster acquisition speed.

3.4 | Homogeneity of the illumination

The illumination inhomogeneity was measured by imaging a Chroma autofluorescence plastic slide, with the 20× and 40× objective in widefield mode, with all the available single band filter cubes (Figure 5). The illumination fields were independent of the objectives used. The center of the illumination is slightly off centered, caused by the special optical system of the microscope. There is an option for using software flatfield correction based on multiple averaged low-pass filtered fields, as well as for the use of calibration flatfield images saved for each different filter set and optical path used by the device. Notably, the calibration images are saved and run separately for the two halves of the camera image to also correct for unevenness caused by other elements of the optical path.

3.5 | Sensitivity and linearity

The signal response of the microscope was determined by using InSpeck green intensity reference beads. As Figure 6A shows, the instrument response is linear in both widefield and confocal mode, R^2 values are 0.9996 and 0.9997, respectively. The sensitivity of the microscope was determined on QIFIKIT beads containing five populations with different numbers of labeled monoclonal antibodies on their surface. Figure 6B shows that in both imaging modes all the five bead populations could be detected. The QIFIKIT average bead diameter is 10 μm, similar to an average cell, hence the detectable epitope numbers that are in the range of 2.000–700.000 can also be applied to cellular samples.

3.6 | Application to large and thick samples

The 3D capabilities of the device are demonstrated using a particularly challenging sample—a cell multilayer grown on a contact lens for transplantation purposes for the treatment of limbal stem cell deficiency. The sample containing mesenchymal-like vimentin positive feeder cells and epithelial cells differentiating in CK19 and CK3 positive directions has been labeled for these three proteins as well as nuclear DNA and imaged in confocal mode through its full thickness which is considerable (50 μm) given the curvature of the contact lens substrate. Figure 7A shows an extended depth of focus overview of a quarter contact lens with a marginal area where CK3 positive differentiated cells (green) abound. A ROI from this area is shown in close-up as digitized by the Pannoramic scanner (Figure 7B) and for reference as seen with the LSM 880 confocal (Figure 7C). Line intensity profiles from a specific area in the ROI where foreground and background could be compared show that contrast and detail in the Pannoramic scanner is comparable or somewhat better under the applied acquisition settings. Wide field imaging and aperture correlated confocality give the pathology scanner a clear time advantage, voxel time being below 1 μs as opposed to several 10 μs in the LSM. Navigation in the digital slide is demonstrated in Video S2.

4 | CONCLUSIONS

The performance of the Pannoramic Confocal is comparable to that of laser scanning confocal microscopes, providing sensitive and precise quantitative detection in brightfield transmission imaging as well as in multispectral widefield and confocal fluorescence. 3D deconvolution using actual system PSF can also be performed and further improves confocal image quality. Since confocal fluorescence detection is implemented in a digital pathology scanner, high speed scanning of large samples, analysis of tissue heterogeneity or molecular gradients, and detection of rare events are inherent features that are not readily available in a conventional LSM.

Confocality in fluorescence-based histopathology offers the advantage of separating signals that vertically overlap even in a sample of normal thickness, for example, when counting FISH probes [6]. By

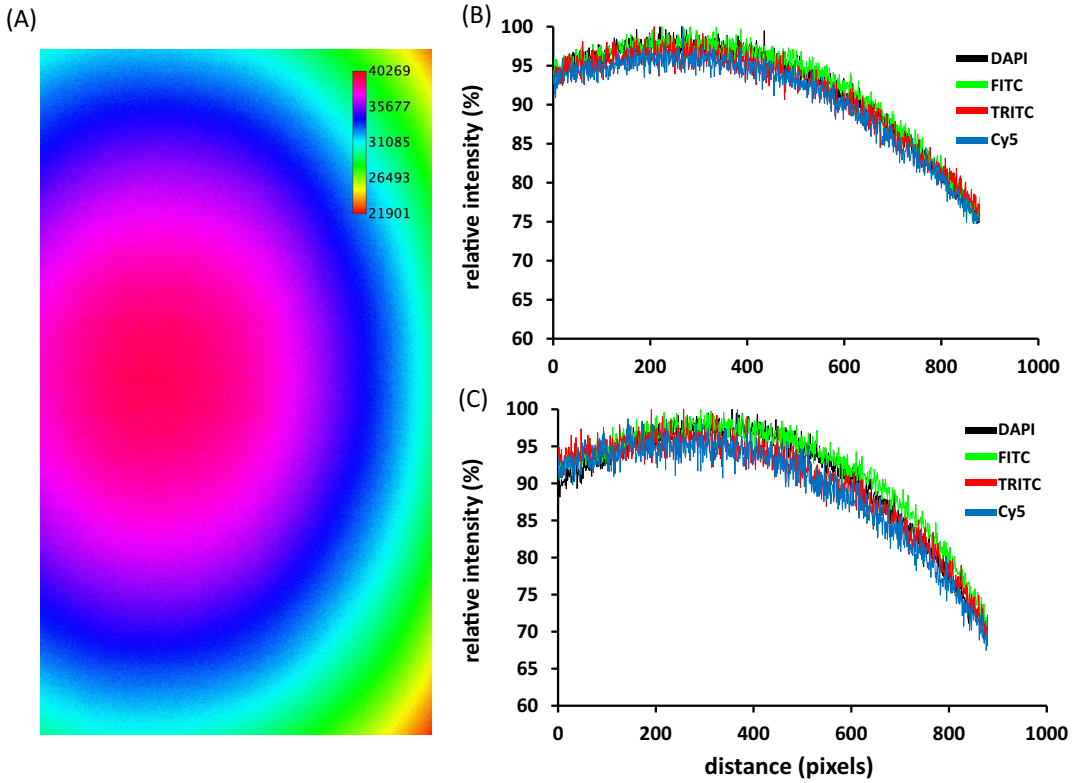

FIGURE 5 Homogeneity of illumination. (A) Fluorescence of flatfield standard slide (20× objective, DAPI channel, widefield). (B) Intensity profiles with the 20× objective for the four major spectral channels. (C) Intensity profiles with the 40× objective for the four major spectral channels [Color figure can be viewed at wileyonlinelibrary.com]

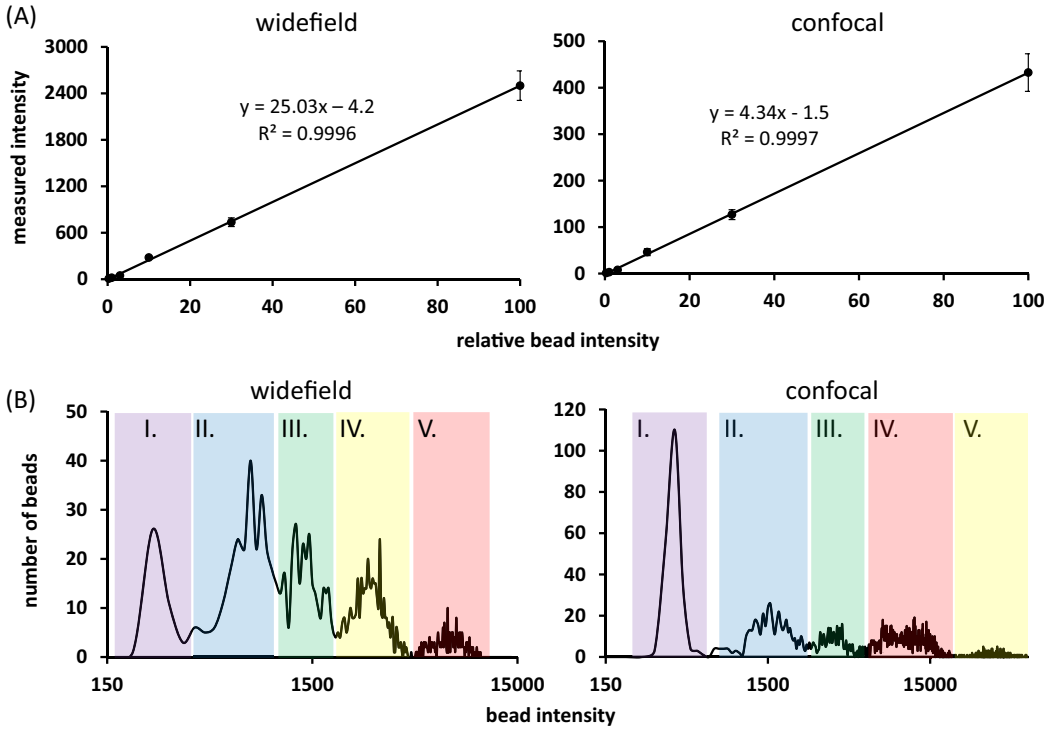

FIGURE 6 Linearity and sensitivity. (A) Linearity of instrument response measured with InSpeck green linearity calibration beads using the 20× objective in widefield and confocal mode. Mean intensity ± SD, for every population at least 30 beads are plotted. (B) Sensitivity of the instrument in widefield and confocal mode assessed with Alexa Fluor 488-conjugated secondary antibodies bound to mouse Fc on QIFIKIT beads. The intensity distribution histogram is plotted for 1190 beads (widefield) or 3196 beads (confocal). The number of Fc target molecules on the five bead populations is the following. I: 2200; II: 14,000; III: 48,000; IV: 169,000; V: 724,000 [Color figure can be viewed at wileyonlinelibrary.com]

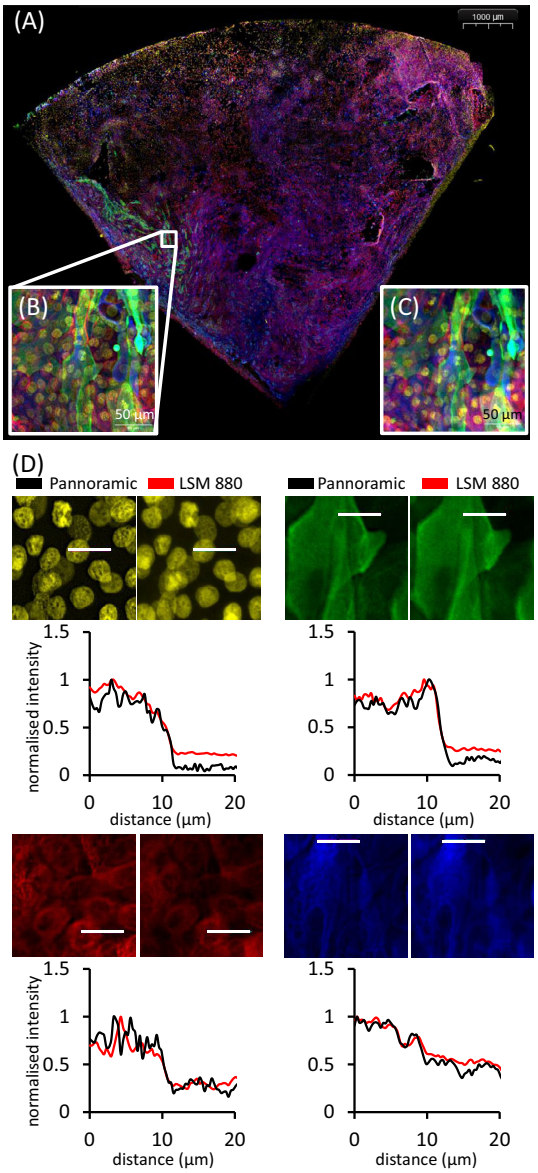

FIGURE 7 Applicability for multispectral imaging of large samples. Corneal limbal explants grown into cell multilayers on contact lenses were labeled for vimentin (red), cytokeratin 3 (green), cytokeratin 19 (blue), and nuclear DNA (yellow). For whole slide scanning in autofocus mode, exposure times were 300, 40, 20, and 20 ms in the DAPI, FITC, TRITC, and Cy5 channel, respectively. Twenty-five confocal slices 2 µm apart have been acquired using the 20× objective. The 1.14 cm^2 area composed of 63,100 tiles was imaged in 7 h 18 min 36 s, contains 2.71 × 10^{10} voxels in each of the four color channels at 16-bit depth and is stored with lossless compression in a 78.4 GB proprietary MRXS file. Cumulative voxel time including post processing for flatfield correction and stitching was 0.97 µs. (A) Extended depth of focus image of the whole mount sample. (B) Confocal slice from the ROI overlaid in panel A. (C) Same ROI as in (B), imaged with an LSM 880, using a 40× water immersion objective. Video S2 shows navigation in the sample and the ROI displayed in (B) and (C). (D) An identical area in both ROIs in (B) and (C) was splitted into channels and 20 µm long normalized intensity profiles along the indicated lines were plotted after maximizing the overlap between the areas along the x axis. [Color figure can be viewed at wileyonlinelibrary.com]

extension, the now evolving multiplex spatial phenotyping approaches (e.g., PhenoCycler by Akoya Biosciences) require confocality to avoid misallocation of phenotypes owed to overlaps along the *z* axis. As a next step, application to thick sections can be foreseen, where, in addition to avoiding z-overlaps, the added diagnostic value of extended sampling can lead to better appreciating rare events and spatial heterogeneity besides opening a window on 3D morphology.

Thereby, the Pannoramic Confocal opens up new ways for analyzing tissue sections, organoid cultures or large numbers of adherent cells. We propose that its features will equally appeal to users doing advanced pathological diagnostics, research on clinical samples, or on preclinical in vitro or ex vivo tissue models.

ACKNOWLEDGMENT

We acknowledge the financial support from GINOP-2.2.1-15-2017-00072 (co-financed by the Hungarian State and the European Regional Development Fund) and OTKA K135938 (the National Research, Development and Innovation Office, Hungary).

CONFLICT OF INTEREST

Géza Antalffy and Béla Molnár are affiliated with 3DHistech Ltd.

PEER REVIEW

The peer review history for this article is available at https://publons.com/publon/10.1002/cyto.a.24675.

ORCID

György Vereb https://orcid.org/0000-0003-2157-3265

REFERENCES

1. Barisoni L, Lafata KJ, Hewitt SM, Madabhushi A, Balis UGJ. Digital pathology and computational image analysis in nephropathology. Nat Rev Nephrol. 2020;16(11):669–85.
2. Hamilton PW, Bankhead P, Wang Y, Hutchinson R, Kieran D, McArt DG, et al. Digital pathology and image analysis in tissue biomarker research. Methods. 2014;70(1):59–73.
3. Jahn SW, Plass M, Moinfar F. Digital pathology: advantages, limitations and emerging perspectives. J Clin Med. 2020;9(11):3697.
4. Fraggetta F et al. Best practice recommendations for the implementation of a digital pathology workflow in the anatomic pathology laboratory by the European Society of Digital and Integrative Pathology (ESDIP). Diagnostics (Basel). 2021;11(11):2167.
5. Cheng C, Reis SA, Adams ET, Fass DM, Angus SP, Stuhlmiller TJ, et al. High-content image-based analysis and proteomic profiling identifies tau phosphorylation inhibitors in a human iPSC-derived glutamatergic neuronal model of tauopathy. Sci Rep. 2021;11(1):17029.
6. Frankenstein Z, Uraoka N, Aypar U, Aryeequaye R, Rao M, Hameed M, et al. Automated 3D scoring of fluorescence in situ hybridization (FISH) using a confocal whole slide imaging scanner. Appl Microsc. 2021;51(1):4.
7. Toth E et al. Limbal and conjunctival epithelial cell cultivation on contact lenses-different affixing techniques and the effect of feeder cells. Eye Contact Lens. 2017;43(3):162–7.
8. Zsebik B, Ujlaky-Nagy L, Losonczy G, Vereb G, Takács L. Cultivation of human Oral mucosal explants on contact lenses. Curr Eye Res. 2017;42(8):1094–9.
9. Theer P, Mongis C, Knop M. PSFj: know your fluorescence microscope. Nat Methods. 2014;11(10):981–2.

10. Tinevez JY, Perry N, Schindelin J, Hoopes GM, Reynolds GD, Laplantine E, et al. TrackMate: an open and extensible platform for single-particle tracking. Methods. 2017;115:80–90.

SUPPORTING INFORMATION

Additional supporting information can be found online in the Supporting Information section at the end of this article.

How to cite this article: Rebenku I, Bartha FA, Katona T, Zsebik B, Antalffy G, Takács L, et al. Taking molecular pathology to the next level: Whole slide multicolor confocal imaging with the Pannoramic Confocal digital pathology scanner. Cytometry. 2022. https://doi.org/10.1002/cyto.a.24675